JOURNAL OF CHEMICAL INFORMATION AND MODELING

Article

pubs.acs.org/jcim

Density Functional Theory and Electrochemical Studies: Structure–Efficiency Relationship on Corrosion Inhibition

Rosa L. Camacho-Mendoza,[†] Evelin Gutiérrez-Moreno,[†] Edmundo Guzmán-Percástegui,[†] Eliazar Aquino-Torres,[†] Julián Cruz-Borbolla,[*,†] José A. Rodríguez-Ávila,[†] José G. Alvarado-Rodríguez,[†] Oscar Olvera-Neria,[‡] Pandiyan Thangarasu,[§] and José L. Medina-Franco[§]

[†]Área Académica de Química, Universidad Autónoma del Estado de Hidalgo, Unidad Universitaria, km 4.5 Carretera Pachuca-Tulancingo, C.P. 42184, Pachuca-Hidalgo, México

[‡]Área de Física Atómica Molecular Aplicada (FAMA), CBI, Universidad Autónoma Metropolitana-Azcapotzalco, Av. San Pablo 180, Col. Reynosa, Mexico City, C.P. 02200, México

[§]Facultad de Química, Universidad Nacional Autónoma de México, Ciudad Universitaria, Mexico City, C.P. 04510, México

Supporting Information

ABSTRACT: The relationship between structure and corrosion inhibition of a series of 30 imidazol, benzimidazol, and pyridine derivatives has been established through the investigation of quantum descriptors calculated with PBE/6-311++G**. A quantitative structure–property relationship model was obtained by examination of these descriptors using a genetic functional approximation method based on a multiple linear regression analysis. Our results indicate that the efficiency of corrosion inhibitors is strongly associated with aromaticity, electron donor ability, and molecular volume descriptors. In order to calibrate and validate the proposed model, we performed electrochemical impedance spectroscopy (EIS) studies on imidazole, 2-methylimidazole, benzimidazole, 2-chloromethylbenzimidazole, pyridine, and 2-aminopyridine compounds. The experimental values for efficiency of corrosion inhibition are in good agreement with the estimated values obtained by our model, thus confirming that our approach represents a promising and suitable tool to predict the inhibition of corrosion attributes of nitrogen containing heterocyclic compounds. The adsorption behavior of imidazole or benzimidazole heterocyclic molecules on the Fe(110) surface was also studied to elucidate the inhibition mechanism; the aromaticity played an important role in the adsorbate–surface complex.

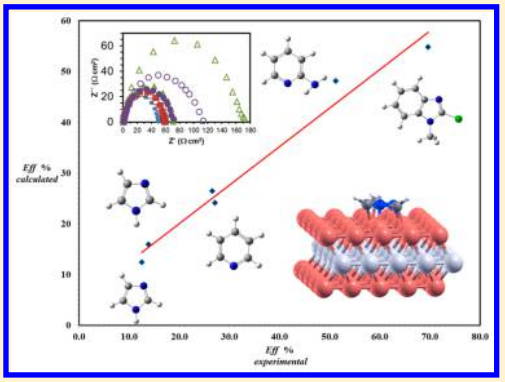

INTRODUCTION

Over the last decades, the design and construction of novel systems that efficiently inhibits corrosion onto metallic surfaces has gained much attention.[1−4] Progress in this field has shown that corrosion inhibition is influenced by several factors such as the nature and state of the metallic surface, the type of corrosive medium, and the structure of the chemical compound used as inhibitor which is directly related to their adsorption efficiency onto the metal surface.[1−4] These studies have revealed that quantum chemical descriptors such as molecular orbital energies, frontier orbital energy gap $E_{HOMO}-E_{LUMO}$ (where HOMO = highest occupied molecular orbital and LUMO = lowest unoccupied orbital), atomic charges, and dipole moments are key properties associated with the corrosion inhibition of chemical compounds.[1−15]

Structure–activity relationships (SARs) or, more generally, structure–property relationships (SPRs) have proven to be versatile tools to study either chemical or biological systems. Qualitative SAR/SPR or quantitative (QSPR/QSAR) models have allowed extensive developments in drug design, pharmaceutical and agrochemical industry, food chemistry, cosmetics, and nanotechnology.[16−27] Although the development of QSPR methodology has been extended to the study of corrosion phenomenon,[28−31] the design of reliable statistical models usually faces multicollinearity, overfitting, and spurious variables. To overcome these inconveniences, Todeschini and co-workers have proposed auxiliary rules[32−35] to obtain suitable mathematical models with predictive ability by using a minimum number of variables. For example, a fundamental statistical rule considers that the number of descriptors must not exceed the sample size; this rule is given by the $3p < n$ relation, where p is the number of descriptors and n is the number of samples (e.g., molecules). Interestingly, this rule may be of great benefit to the final model; on the other hand, in some studies where this rule was not applied resulted in nonpredictive models when an external validation of the corrosion inhibition efficiency (hereafter, eff %) was performed.[28,30,31]

Received: June 17, 2015
Published: October 27, 2015

DOI: 10.1021/acs.jcim.5b00385
J. Chem. Inf. Model. 2015, 55, 2391−2402

In this context and given the environment-friendly character as well as their extensive use in pharmaceutical and chemical industry,[36,37] nitrogen-based heterocycles such as imidazole, benzimidazole, and pyridine derivatives have been recently employed as corrosion inhibitors for mild steel under acidic HCl medium.[38−40] Considering these achievements, a statistically adequate QSPR model of predictive attributes for nitrogen-based heterocycles becomes highly desirable. Herein, we present a mathematical approach that predicts the corrosion inhibition of imidazole, benzimidazole and pyridine derivatives with great efficiency. Our model has been developed based on a QSPR study that applies the rules proposed by Todeschini. In order to validate and calibrate the best mathematical model, we carried out experimental studies by electrochemical impedance spectroscopy on electrodes soaked with solutions of selected nitrogen heterocycles; the experimental results are consistent with the predicted data. Additionally, we performed DFT calculations to study the adsorption behavior of imidazole and benzimidazole molecules on a Fe(110) surface as representative cases to gain greater insights into the mechanism of corrosion inhibition.

COMPUTATIONAL PROCEDURE

The optimization calculations were performed on 30 heterocyclic aromatic molecules, including derivatives of pyridine, imidazole, and benzimidazole. We used the density functional theory (DFT) with three functionals: the Perdew, Burke, and Ernzerhof (PBE)[41,42] exchange correlation functional, the Becke's three-parameter hybrid[43] (B3LYP) functional, and the hybrid functional of Truhlar and Zhao[44] (M06); in all cases we used the 6-31G* and 6-311++G** orbital basis set for all atoms using the Gaussian 09 program (Rev. A 02).[45] It is worth mentioning that this DFT functional−basis set combination has yielded reliable and consistent results in a wide variety of chemical systems.[46] All molecules were optimized both in gas and aqueous phases; for the total optimization in water as solvent, we employed the integral equation formalism polarizable continuum model (IEFPCM). Second derivation was applied to each calculation in order to corroborate a minimum on the potential energy surface. A number of chemical descriptors such as E_{HOMO}, E_{LUMO}, hardness (η), electrophilicity (ω), potential ionization (I), dipole momentum (μ_D), atomic charges (q), proton affinities (PA), partition coefficient (Log P), and anisotropy (bq_{ANS}) were considered as indicators of chemical reactivity. The nucleus−independent chemical shifts (NICS) data were obtained by means of a single-point calculation in a system formed by a test charge positioned 1 Å from the ring critical point (RCP) of the aromatic molecule;[47,48] the RCP was calculated according to the Atoms in Molecules (AIM) theory.[49] The harmonic oscillator model of aromaticity index (HOMA) and the molecular volume (V) were obtained with the Multiwfn software.[50] The HOMA was obtained from the sum of the contributions of all bonds in the ring; a HOMA value close to 1 is associated with aromatic molecules; whereas, a 0 value indicates nonaromatic character.[51]

Several mathematical polynomial multiple regression models were obtained for descriptors by using MobyDigs software based on the strategy developed by Todeschini et al.[32−35] The model was constructed and validated by using a training set of 25 molecules and a test set of five compounds, namely imidazole, benzimidazole, 2-aminobenzimidazole, pyridine, and 2,4,6-trimethylpyridine. Furthermore, the theoretical model was validated with external experimental data generated in this study.

The Vienna Ab Initio Simulation package (VASP 5.4.1)[52,53] was used to study the adsorption of imidazole and benzimidazole molecules on the Fe(110) surface. The exchange-correlation energy was included in the PBE functional,[41,42] within the generalized gradient approximation (GGA). The electron−ionic core interaction was represented by the projector-augmented-wave potentials (PAW)[54,55] with $3d^74s^1$, $2s^22p^2$, and $2s^22p^3$ electrons treated as valence electrons for Fe, C, and N atoms, respectively, with a cutoff energy of 400 eV. The spin polarization calculations were incorporated for Fe bulk and the Fe surface to correct the iron magnetic properties. The calculations were accomplished with (11 × 11 × 11) and (3 × 3 × 1) Monkhorst−Pack, k-points mesh for the bulk and surface, respectively. The convergence criterion was set to the 1×10^{-6} eV for the self-consistent field (SCF). The optimized bulk lattice constant for the body centered cubic (bcc) unit cell was 2.835 Å with a magnetic moment of 2.245 μ_B; these values agree with previous experimental results and PAW−GGA theoretical calculations.[56,57] The Fe(110) surface was modeled using a supercell (5 × 5) with three metal layers and a 16 Å vacuum regions to separate the slabs in the z-direction to accommodate the heterocyclic compounds.

Furthermore, Bader's method[58,59] was used to analyze the charge transfer upon the adsorption of the different adsorbates on Fe(110). The more stable Fe(110) surface was chosen instead of either the less dense Fe (100) or least stable Fe (111) surfaces.[60] An implicit solvation model[61] was used during the adsorption of imidazole and benzimidazole on Fe(110) surface to consider the effects of electrostatics, cavitation, and dispersion on the interaction between the heterocyclic compounds, metal surface, and aqueous phase. This solvation model is implemented into the VASP code.

Electrochemical Procedure. The corrosion inhibition efficiency of imidazole, 2-methylimidazole, benzimidazole, 2-chloromethylbenzimidazole, pyridine, and 2-aminopyridine was studied by using electrochemical impedance spectroscopy (EIS). These compounds were obtained from Sigma−Aldrich (ACS grade, USA). A standard electrochemical cell (50 mL) was assembled with a carbon steel working electrode (WE), a platinum counter electrode (CE), and a saturated Ag/AgCl reference electrode. The carbon steel working electrode was a flat specimen with an exposure area of 0.2 cm^2, which was abraded by using different grades of sandpaper (120−1200). The electrodes were degreased with acetone and then washed with bidistilled water to avoid any carbon pollution. The composition of the carbon steel was 0.18 C, 0.35 Mn, 0.17 Si, 0.025 S, 0.03 P wt%, and the remaining composition content was Fe. The cell was connected to an Autolab PGSTAT 30 potenciostat coupled to a frequency response analyzer (FRA) which was controlled by FRA software (V 2.0). Nitrogen gas was bubbled into an HCl solution (1.0 M) containing the inhibitor (1×10^{-3} M) for 45 min to eliminate any dissolved oxygen in the medium. The inhibitor concentration selected guarantees the formation of a protective film on the electrode interface.[62]

The electrochemical studies were carried out at room temperature under static conditions. All the experiments were performed after dipping the working electrode into HCl (1.0 M) containing the inhibitor at the open-circuit potential, E_{corr}, with respect to the Ag/AgCl reference electrode. Two independent experiments were carried out for each concen-

DOI: 10.1021/acs.jcim.5b00385
J. Chem. Inf. Model. 2015, 55, 2391−2402

	Compound	R^1	R^2	R^3	R^4	R^5
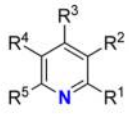	**1**	H	H	H	H	H
	2	H	Me	H	H	H
	3	Me	H	H	H	H
	4	H	OH	H	H	H
	5	H	H	Me	H	H
	6	Me	H	H	H	Me
	7	H	H	OMe	H	H
	8	Cl	H	H	H	H
	9	OH	H	H	H	H
	10	Br	H	H	H	H
	11	Me	H	Me	H	Me
	12	H	H	C(O)Me	H	H
	13	H	H	NMe_2	H	H
	14	H	H	CH_2Ph	H	H
	15	OMe	H	H	H	H
	16	H	H	NH_2	H	H
	17	CH_2Ph	H	H	H	H
	18	H	Br	H	Br	H
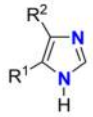	**19**	H	H	-	-	-
	20	Me	H	-	-	-
	21	CH_2OH	H	-	-	-
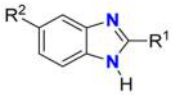	**22**	H	H	-	-	-
	23	Me	H	-	-	-
	24	H	NO_2	-	-	-
	25	H	C(O)OH	-	-	-
	26	NH_2	H	-	-	-
	27	Py-N	H	-	-	-
	28	CH_2Ph	H	-	-	-
	29	C_6H_4-2-NH_2	H	-	-	-
	30	Ph	H	-	-	-

Figure 1. Chemical structures of the studied compounds.

tration. EIS was recorded between 10 kHz and 10 mHz, with a 15 mV peak-to-peak perturbation. The inhibition efficiencies (eff %) for each tested compound were calculated[63] using the following equation:

$$\text{eff}(\%) = \frac{R_{ct} - R_{ct}^0}{R_{ct}} \times 100 \quad (1)$$

where R_{ct} and R_{ct}^0 are the charge transfer resistance in the presence and absence of the inhibitor, respectively.

Theory and Equations. The reactivity of the heterocyclic compounds was analyzed by the following quantum chemical parameters based on DFT calculations; energy of the highest occupied molecular orbital (E_{HOMO}), energy of the lowest unoccupied molecular orbital (E_{LUMO}), Hirshfeld charges (q),[64] and dipolar moment (μ_D).

First, we calculated the ionization potential (I) and the electronic affinity (A) in a vertical manner[65] applying eqs 2 and 3.

Ionization potential (I)

$$I = E_c^{N-1} - E_o^N \quad (2)$$

Electron affinity (A)

$$A = E_o^N - E_a^{N+1} \quad (3)$$

where E_c^{N-1} = energy after losing one electron (cation); E_o^N = basal state energy (neutral); E_a^{N+1} = energy after gaining one electron (anion).

Electronegativity and hardness[66−68] were obtained from eqs 4 and 5.

Absolute electronegativity

$$\chi = \frac{I + A}{2} \quad (4)$$

Absolute hardness

$$\eta = \frac{I - A}{2} \quad (5)$$

where I corresponds to the ionization potential and A is the electron affinity.

Similarly, we performed calculations on electrophilicity[68] to establish the charge transfer process, i.e., the relationship between the maximum electron transfer and the energy variation, eq 6, where μ is the chemical potential and η is the hardness of the system.

$$\omega \equiv \frac{\mu^2}{2\eta} \quad (6)$$

From the equations it is evident that the chemical reactivity ultimately depends on the electron affinity as well as on the ionization potential.

DOI: 10.1021/acs.jcim.5b00385
J. Chem. Inf. Model. 2015, 55, 2391−2402

Table 1. Descriptors Calculated with PBE/6-311++G for the 30 Heterocyclic Compounds in the Gas Phase**

molecule	eff %	E_{HOMO}	E_{LUMO}	ω	ω^-	ω^+	I	A	η	PA	V	μ_D	Log P	q	bq_{ISO}	bq_{ANS}	HOMA
		eV	eV	eV	eV	eV	eV	eV	eV	eV	A^3	Debye	du	du	du	du	du
(1) pyridine	13	−5.96	−1.91	0.9	4.57	0.29	9.38	−0.82	5.10	9.56	113	2.33	0.68	−0.18	−9.83	−26.82	0.97
(2) 3-methylpyridine	14	−5.85	−1.84	0.94	4.64	0.34	9.22	−0.63	4.92	9.72	136	2.62	1.17	−0.18	−9.73	−25.65	0.96
(3) 2-methylpyridine	19	−5.85	−1.80	1.01	4.81	0.41	9.19	−0.40	4.80	9.78	137	1.91	0.96	−0.18	−9.50	−25.13	0.97
(4) 3-hydroxypyridine	21	−5.95	−1.90	0.85	4.32	0.27	8.88	−0.79	4.83	9.63	124	3.59	0.41	−0.36	−9.58	−24.25	0.97
(5) 4-methylpyridine	24	−5.87	−1.74	1.01	4.81	0.42	9.19	−0.39	4.79	9.77	137	2.88	1.17	−0.19	−9.77	−25.80	0.97
(6) 2,6-dimethylpyridine	26	−5.75	−1.71	0.86	4.33	0.29	8.80	−0.73	4.77	9.96	161	1.46	1.25	−0.19	−9.34	−23.21	0.96
(7) 4-methoxypyridine	28	−5.89	−1.49	0.82	4.25	0.24	8.94	−0.92	4.93	10.11	148	3.44	0.66	−0.31	−9.49	−23.37	0.96
(8) 2-chloropyridine	28	−6.57	−2.23	1.01	4.86	0.41	9.35	−0.45	4.90	9.27	135	3.43	1.55	−0.24	−9.41	−23.78	0.97
(9) 2-hydroxypiridine	29	−5.97	−1.88	0.84	4.31	0.27	8.88	−0.81	4.85	9.21	124	1.35	0.95	−0.39	−8.76	−22.28	0.97
(10) 2-bromopyridine	33	−6.42	0.00	1.01	4.8	0.42	9.14	−0.38	4.76	9.31	143	3.44	1.66	−0.27	−9.32	−23.36	0.97
(11) 2,4,6-trimethylpyridine	38	−5.68	−1.57	0.86	4.29	0.3	8.64	−0.65	4.64	10.11	184	1.99	1.73	−0.19	−8.84	−22.12	0.96
(12) 4-acetylpyridine	49	−6.32	−3.52	1.39	5.68	0.92	8.84	0.69	4.07	9.45	139	2.47	0.42	−0.41	−9.56	−23.85	0.97
(13) 4-dimethylaminopyridine	61	−5.13	−1.14	0.79	3.89	0.29	7.72	−0.52	4.12	10.37	176	4.95	0.84	−0.28	−8.69	−21.75	0.91
(14) 4-benzylpyridine	72	−5.87	−1.82	0.97	4.49	0.44	8.27	−0.18	4.22	9.90	237	2.77	2.65	−0.19	−9.67	−25.28	0.97
(15) 2-methoxypyridine	73	−5.73	−1.72	0.78	4.05	0.23	8.49	−0.86	4.67	9.65	148	0.61	1.20	−0.31	−8.92	−22.23	0.96
(16) 4-aminopyridine	86	−5.62	−1.31	0.86	4.25	0.31	8.46	−0.58	4.52	10.13	131	4.18	−0.07	−0.38	−8.39	−21.08	0.95
(17) 2-benzylpyridine	88	−5.84	−1.87	0.98	4.55	0.44	8.42	−0.21	4.31	9.86	235	1.87	2.66	−0.18	−9.57	−24.94	0.97
(18) 3,5-dibromopyridine	98	−6.55	−2.57	1.14	5.09	0.58	8.98	0.04	4.47	9.17	171	0.86	1.90	−0.33	−9.06	−20.69	0.98
(19) imidazole	18	−5.71	−0.78	0.62	3.74	0.09	8.99	−1.70	5.35	9.67	92	3.78	−0.28	−0.29	−9.87	−27.20	0.88
(20) 5-methylimidazole	20	−5.39	−0.08	0.71	3.86	0.17	8.47	−1.10	4.78	9.88	117	4.06	−0.14	−0.26	−9.85	−28.07	0.87
(21) 4-methyl-5-hydroxymethylimidazole	23	−5.29	−1.10	0.93	4.35	0.41	8.11	−0.23	4.17	10.06	151	3.88	−0.27	−0.42	−9.53	−26.31	0.88
(22) benzimidazole	29	−5.71	−1.59	0.79	4.04	0.25	8.33	−0.75	4.54	9.78	153	3.53	1.35	−0.28	−10.39	−27.47	0.77
(23) 2-methylbenzimidazole	35	−5.53	−1.42	0.78	3.95	0.26	8.07	−0.69	4.38	10.00	176	3.62	1.61	−0.21	−9.88	−23.74	0.77
(24) 5-nitrobenzimidazole	43	−6.48	−3.36	1.44	5.83	0.96	8.98	0.76	4.11	9.11	183	7.97	1.24	−0.43	−10.10	−26.14	0.77
(25) 5-carboxybenzimidazole	66	−6.08	−2.28	1.06	4.8	0.53	8.57	−0.02	4.29	9.60	189	5.71	0.95	−0.67	−9.63	−26.29	0.76
(26) 2-aminobenzimidazole	89	−5.07	−1.14	0.9	4.14	0.42	7.58	−0.14	3.86	9.74	170	3.95	1.14	−0.68	−8.16	−18.67	0.74
(27) 2-pyridylbenzimidazole	93	−5.78	−2.75	1.29	5.2	0.87	7.97	0.69	3.64	9.78	247	3.65	2.12	0.03	−9.29	−21.61	0.78
(28) 2-benzyl-benzimidazole	93	−5.50	−1.66	0.94	4.28	0.44	7.76	−0.09	3.93	10.13	276	3.67	3.31	0.00	−9.99	−24.75	0.77
(29) 2-(ortho-aminophenyl)-benzimidazole	94	−5.20	−2.10	0.97	4.24	0.54	7.23	0.18	3.52	10.23	268	4.09	2.52	−0.27	−11.29	−23.57	0.78
(30) 2-phenylbenzimidazole	95	−5.41	−2.29	1.06	4.52	0.61	7.52	0.29	3.61	10.06	252	3.08	3.27	0.01	−9.03	−21.01	0.78

DOI: 10.1021/acs.jcim.5b00385
J. Chem. Inf. Model. 2015, 55, 2391−2402

Table 2. Descriptors Calculated with PBE/6-311++G for the 30 Heterocyclic Compounds in the Aqueous Phase**

molecule	eff %	E_{HOMO}	E_{LUMO}	ω	ω^-	ω^+	I	A	η	PA	V	μ_D	Log P	q	bq_{ISO}	bq_{ANS}	HOMA
		eV	eV	eV	eV	eV	eV	eV	eV	eV	A^3	Debye	du	du	du	du	du
(1) pyridine	13	−6.21	−1.98	1.62	5.77	1.43	7.27	1.43	2.92	11.71	113	3.18	0.68	−0.22	−9.83	−26.82	0.97
(2) 3-methylpyridine	14	−6.13	−1.94	1.74	6.40	1.43	8.53	1.41	3.56	11.76	137	3.60	1.17	−0.22	−9.72	−25.61	0.96
(3) 2-methylpyridine	19	−6.12	−1.92	1.57	5.60	1.38	7.05	1.38	2.83	11.82	137	2.74	0.96	−0.21	−9.50	−25.18	0.96
(4) 3-hydroxypyrydine	21	−5.98	−1.97	1.56	5.48	1.41	6.71	1.41	2.65	11.69	124	4.90	0.41	−0.40	−9.56	−24.26	0.96
(5) 4-methylpyridine	24	−6.17	−1.84	1.55	5.60	1.33	7.21	1.32	2.94	11.79	137	3.95	1.17	−0.22	−9.52	−25.35	0.96
(6) 2,6-dimethylpyridine	26	−6.03	−1.85	1.53	5.45	1.35	6.85	1.35	2.75	11.86	161	2.23	1.25	−0.21	−9.36	−23.30	0.96
(7) 4-methoxypyridine	28	−6.20	−1.62	1.39	5.15	1.13	6.92	1.11	2.90	11.85	148	4.65	0.66	−0.35	−9.52	−25.35	0.96
(8) 2-chloropyridine	28	−6.62	−2.21	1.77	6.11	1.66	7.27	1.65	2.81	11.34	135	4.71	1.55	−0.30	−9.55	−24.12	0.98
(9) 2-hydroxypiridine	29	−6.05	−1.94	1.55	5.47	1.39	6.76	1.39	2.68	11.42	124	1.86	0.95	−0.41	−8.88	−22.58	0.97
(10) 2-bromopyridine	33	−6.52	−2.23	1.78	6.09	1.69	7.13	1.67	2.73	11.35	142	4.75	1.66	−0.32	−9.45	−23.75	0.97
(11) 2,4,6-trimethylpyridine	38	−6.00	−1.72	1.45	5.26	1.25	6.78	1.25	2.76	11.94	184	2.97	1.73	−0.22	−8.82	−22.12	0.95
(12) 4-acetylpyridine	49	−6.18	−3.25	2.72	8.12	3.30	6.95	2.68	2.13	11.57	162	3.48	0.42	−0.47	−9.92	−24.55	0.96
(13) 4-dimethylaminopyridine	61	−5.14	−1.32	1.12	4.19	0.88	5.75	0.86	2.45	12.12	176	7.05	0.84	−0.32	−8.41	−21.13	0.88
(14) 4-benzylpyridine	72	−6.14	−2.00	1.69	5.75	1.64	6.60	1.62	2.49	11.81	237	3.72	2.41	−0.22	−13.17	−27.48	0.96
(15) 2-methoxypyridine	73	−5.86	−1.84	1.47	5.22	1.30	6.53	1.30	2.61	11.67	148	1.00	1.20	−0.34	−9.00	−22.44	0.95
(16) 4-aminopyridine	86	−5.60	−1.41	1.22	4.59	0.97	6.29	0.94	2.68	12.04	130	5.96	−0.07	−0.41	−8.17	−20.49	0.93
(17) 2-benzylpyridine	88	−6.07	−1.99	1.68	5.71	1.62	6.57	1.60	2.48	11.75	236	2.64	2.66	−0.21	−9.54	−24.95	0.97
(18) 3,5-dibromopyridine	98	−6.48	−2.49	1.98	6.50	2.04	6.98	1.94	2.52	11.32	171	1.25	2.18	−0.35	−9.13	−20.84	0.98
(19) imidazole	18	−5.82	−0.62	1.27	4.80	1.00	6.65	0.96	2.85	11.81	93	5.08	−0.28	−0.27	−10.68	−31.73	0.89
(20) 5-methylimidazole	20	−5.51	−0.54	1.23	4.60	0.98	6.29	0.95	2.67	11.88	117	5.53	−0.14	−0.28	−9.90	−28.27	0.88
(21) 4-methyl-5-hydroxymethylimidazole	23	−5.58	−0.95	1.30	4.55	1.20	5.52	1.19	2.16	11.88	152	5.53	−0.31	−0.53	−9.92	−27.22	0.88
(22) benzimidazole	29	−5.84	−1.71	1.45	5.15	1.30	6.41	1.30	2.55	11.72	156	5.01	1.35	−0.27	−10.64	−28.06	0.79
(23) 2-methylbenzimidazole	35	−5.71	−1.58	1.35	4.89	1.17	6.28	1.16	2.56	11.81	177	5.28	1.61	−0.27	−10.11	−24.36	0.78
(24) 5-nitrobenzimidazole	43	−6.35	−3.64	3.05	8.82	3.89	6.92	2.94	1.99	11.28	183	11.03	−0.76	−0.46	−10.06	−25.79	0.78
(25) 5-carboxybenzimidazole	66	−6.11	−2.45	2.00	6.45	2.12	6.67	1.98	2.34	11.58	189	8.05	0.95	−0.71	−10.48	−26.61	0.78
(26) 2-aminobenzimidazole	89	−5.16	−1.29	1.24	4.46	1.07	5.71	1.07	2.32	11.51	171	6.18	1.14	−0.47	−8.31	−19.43	0.76
(27) 2-pyridylbenzimidazole	93	−5.83	−2.81	2.46	7.33	2.98	6.29	2.43	1.93	11.59	246	5.45	2.12	−0.41	−9.54	−22.23	0.80
(28) 2-benzyl-benzimidazole	93	−5.75	−1.73	1.53	5.28	1.45	6.23	1.44	2.39	11.79	277	5.03	3.31	−0.27	−8.13	−24.33	0.78
(29) 2-(ortho-aminophenyl)-benzimidazole	94	−5.27	−2.22	1.89	5.92	2.13	5.67	1.89	1.89	11.79	267	6.24	2.52	−0.41	−11.50	−24.16	0.79
(30) 2-phenylbenzimidazole	95	−5.57	−2.40	2.06	6.37	2.35	5.99	2.06	1.97	11.72	252	4.84	3.27	−0.24	−9.29	−21.55	0.79

DOI: 10.1021/acs.jcim.5b00385
J. Chem. Inf. Model. 2015, 55, 2391−2402

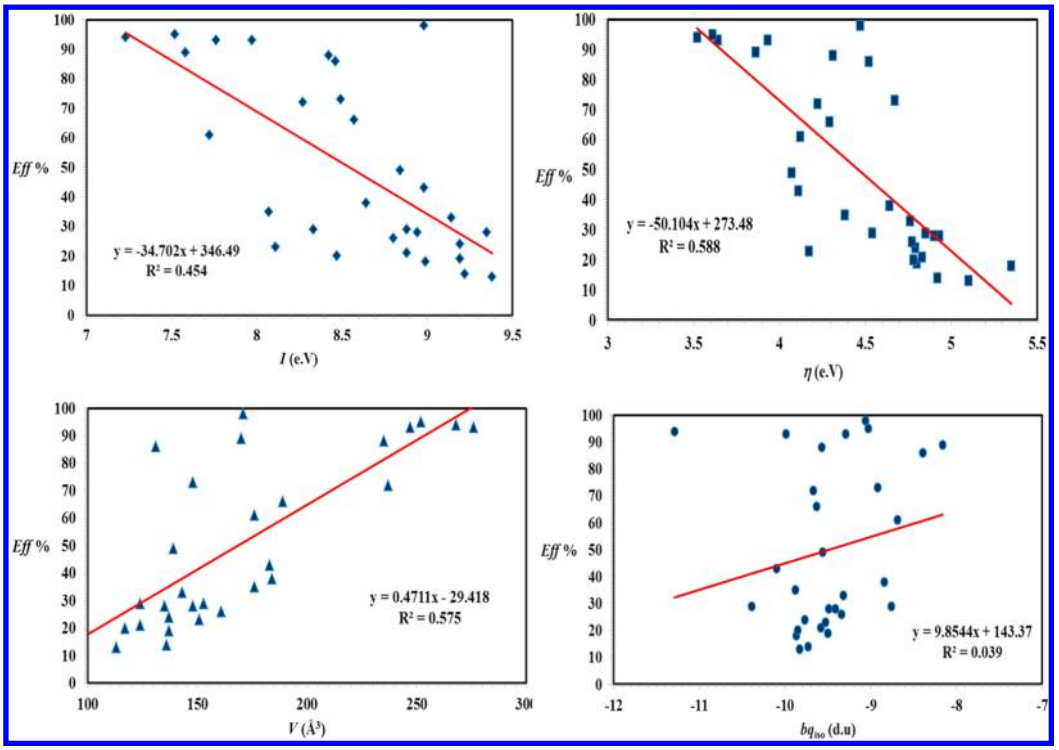

Figure 2. Simple linear regression of some descriptors versus eff %.

Now, in the study of corrosion phenomena, there are two descriptors that have been related to the capability of a chemical species to either donate or accept charge; eqs 7 and 8 were employed to calculate these capabilities.[69]

Electron donor capability

$$\omega^{-} = \frac{(3I + A)^2}{16(I - A)} \tag{7}$$

Electron acceptor capability

$$\omega^{+} = \frac{(I + 3A)^2}{16(I - A)} \tag{8}$$

We calculated the proton affinity (PA) for the reaction A + H^+ → AH^+, which is defined as negative of the reaction enthalpy at 298.15 K; A is each of the studied compounds.[70,71]

The interaction energy between the Fe(110) surface and the imidazole and benzimidazole molecule in aqueous solution is different from that in vacuum. The adsorption energy is defined as[72,73]

$$E_{ads}^{sol} = E_{ads}^{vac} + E_{sol} \tag{9}$$

Where E_{ads}^{vac} is the adsorption energy in vacuum conditions, which can be calculated as follows

$$E_{ads}^{vac} = E_{Fe/mol}^{vac} - E_{Fe}^{vac} - E_{mol}^{vac} \tag{10}$$

Where $E_{Fe/mol}^{vac}$ is the total energy of the Fe(110) surface and the heterocyclic molecule, E_{Fe}^{vac} is the total energy of the Fe(110) surface, and E_{mol}^{vac} is the total energy of the isolated heterocyclic molecule calculated in the box.

E_{sol} is the solvation energy, which can be calculated as

$$E_{sol} = E_{Fe/mol}^{sol} - E_{Fe/mol}^{vac} \tag{11}$$

where $E_{Fe/mol}^{sol}$ is the total energy of the Fe(110) and the heterocyclic molecule in aqueous solution, while $E_{Fe/mol}^{vac}$ is the total energy in vacuum.

RESULTS AND DISCUSSION

The chemical structures used in this study are presented in Figure 1. In order to obtain a reliable model of structure−efficiency relationship on corrosion inhibition, we used the experimental efficiencies of inhibition-to-corrosion data of 30 molecules previously reported.[7,74] First, all molecules were optimized in gas phase with PBE/6-311++G**, M06/6-311++G**, B3LYP/6-311++G**, PBE/6-31G*, M06/6-31G*, and B3LYP/6-31G*. All the calculated structural parameters for this type of heterocyclic compounds, regardless the functional/basis used, are essentially identical to those reported in the literature.[75−77] Taking into account these results, we only listed the structural data obtained from the PBE/6-311++G** in the Supporting Information (Tables S1a−S1c). The descriptors considered to interpret the efficiency of corrosion inhibition were also calculated with all methods; they are listed in Tables 1 and 2 for PBE/6-311++G**, while the results obtained using other methods are listed in the Supporting Information (Tables S2a−S2e). It is noteworthy that the trends in the values of the descriptors do not change notwithstanding the used method.

Now, on the basis of some studies where has been reported the influence of certain properties[78,79] such as E_{LUMO}−E_{HOMO} gap or the aromaticity in the inhibition corrosion processes, our first approach was to analyze the effect of the structural parameters (bond distances and bond angles, molecular volume, number of heteroatoms, partition coefficient), electronic properties (E_{HOMO}, E_{LUMO}, hardness, electrophilicity, potential ionization, dipole momentum, atomic charges), and aromaticity (nucleus−independent chemical shifts, harmonic oscillator model of aromaticity index, anisotropy) of the 30

DOI: 10.1021/acs.jcim.5b00385
J. Chem. Inf. Model. 2015, 55, 2391−2402

Table 3. Correlation Coefficient Matrix

	eff %	E_{HOMO}	E_{LUMO}	Log*P*	*V*	μ_D	*q*	bq_{ISO}	bq_{ANS}	HOMA	ω	ω^+	ω^-	*I*	*A*	η	PA
eff %	1.0	0.2	−0.2	0.6	0.8	0.0	0.1	0.2	0.6	−0.4	0.3	0.1	0.4	−0.7	0.6	−0.8	0.2
E_{HOMO}		1.0	***0.7***	−0.1	0.2	0.1	0.0	0.0	0.1	−0.4	***-0.6***	***-0.7***	−0.4	***-0.7***	−0.2	−0.3	***0.8***
E_{LUMO}			1.0	−0.3	−0.2	−0.1	0.0	0.2	−0.1	0.0	***-0.9***	***-0.9***	***-0.8***	−0.3	***-0.7***	0.3	***0.6***
Log *P*				1.0	***0.9***	−0.2	***0.5***	−0.2	0.3	−0.3	0.3	0.2	0.3	−0.4	***0.5***	***-0.5***	0.1
V					1.0	0.1	0.4	−0.2	0.3	***-0.5***	0.3	0.1	0.4	***-0.7***	***0.6***	***-0.8***	0.4
μ_D						1.0	−0.3	−0.3	−0.2	***-0.6***	0.2	0.1	0.3	−0.2	0.3	−0.3	0.1
q							1.0	−0.2	−0.1	0.1	0.0	0.0	0.0	−0.1	0.0	−0.1	0.3
bq_{ISO}								1.0	***0.7***	0.3	−0.1	−0.1	−0.1	0.0	−0.1	0.1	0.0
bq_{ANS}									1.0	0.0	0.1	0.0	0.2	−0.4	0.3	−0.4	0.1
HOMA										1.0	−0.1	0.1	−0.3	***0.7***	−0.4	***0.6***	***-0.2***
ω											1.0	***1.0***	***1.0***	0.1	***0.9***	***-0.5***	−0.4
ω^+												1.0	***0.9***	0.4	***0.8***	−0.2	***-0.6***
ω^-													1.0	−0.1	***1.0***	***-0.7***	−0.3
I														1.0	−0.3	***0.8***	***-0.6***
A															1.0	***-0.8***	−0.2
η																1.0	−0.3
PA																	1

Table 4. Multiple Linear Regression Models in the Gas Phase (gm_i)

model	model variables	R^2 [a]	R_{ADJ}^2 [b]	$\delta K = 0.1$ [c]	$\delta Q = 0$ [d]	$R^P = 0.05$ [e]	$R^N - t^N = (0.02)$ [f]	Q_{boot} [g]	accepted?
gm_1	E_{HOMO}, E_{LUMO}, *V*, *q*, bq_{ANS}, μ_D, ω, ω^-	82.8	76.3	***0.042***	0.047	***0.03***	***−0.164(−0.103)***	***48.5***	no
gm_2	E_{HOMO}, E_{LUMO}, *V*, *q*, bq_{ANS}, *I*	80.3	75.2	***0.067***	0.031	***0.021***	−0.100 (−0.144)	61.9	no
gm_3	E_{HOMO}, *V*, *q*, bq_{ANS}, *I*	79.2	74.8	***0.080***	0.024	***0.023***	−0.146 (−0.178)	65.1	no
gm_4	*V*, *q*, bq_{ISO}, bq_{ANS}, η	78.4	74.9	***0.070***	0.024	***0.012***	−0.133 (−0.177)	59.4	no
gm_5	Log *P*, *V*, *q*, bq_{ANS}	77.7	74.2	***0.085***	0.012	***0.033***	−0.183 (−0.227)	65.9	no
gm_6	E_{LUMO}, *V*, *q*, bq_{ANS}	77.4	73.8	0.141	0.021	0.079	***−0.252 (−0.227)***	65.5	no
gm_7	*V*, *q*, bq_{ISO}	75.5	72.7	0.11	***−0.002***	0.184	***−0.370 (−0.310)***	65.3	no
gm_8	*V*, bq_{ANS}, ω^-	75.0	71.5	0.183	0.001	0.094	0.000 (−0.310)	61.8	yes
gm_9	E_{HOMO}, bq_{ISO}, *I*	72.3	69.1	***0.022***	***−0.028***	0.312	−0.237 (−0.310)	58.8	no
gm_{10}	μ_D, *V*	66.4	62.5	0.110	***−0.004***	0.097	***−0.322 (−0.309)***	51.5	no

[a] R^2. [b] R_{adj}^2. [c] $K_{XY} - K_X > \delta K = 0.1$. [d] $Q_{LOO}^2 - Q_{ASYM}^2 > \delta Q = 0$. [e] $t^P > R^P = 0.05$. [f] $R^N > t^N(0.02)$. [g] $Q_{boot} > 50\%$.

Table 5. Multiple Linear Regression Models in the Aqueous Phase (am_i)

model	model variables	R^2 [a]	R_{ADJ}^2 [b]	$\delta K = 0.1$ [c]	$\delta Q = 0$ [d]	$R^P = 0.05$ [e]	$R^N - t^N = (0.02)$ [f]	Q_{boot} [g]	accepted?
am_1	E_{LUMO}, *V*, Log *P*, *q*, bq_{ANS}, ω^-	78.8	73.3	***0.039***	***−0.022***	***0.017***	0.000(−0.144)	***47.3***	no
am_2	*V*, bq_{ANS}, ω^+	76.4	73.4	0.235	***−0.003***	0.128	−0.169 (−0.311)	64.71	no
am_3	E_{LUMO}, *V*, *q*, bq_{ANS}, *A*	77.7	73.0	***0.077***	***−0.026***	***0.047***	0.000 (−0.177)	53.13	no
am_4	E_{LUMO}, *V*, bq_{ANS}, *A*	76.0	72.2	***0.087***	***−0.009***	0.059	0.000 (−0.227)	55.37	no
am_5	*V*, *q*, *I*, bq_{ANS}	75.9	72.0	0.141	***−0.025***	***0.042***	0.000 (−0.227)	59.24	no
am_6	*V*, *I*, PA, bq_{ANS}	75.5	71.6	0.138	***−0.043***	***0.041***	−0.157 (−0.227)	57.37	no
am_7	*V*, *q*, bq_{ANS}	74.8	71.9	0.223	***−0.027***	0.087	−0.073 (−0.310)	61.73	no
am_8	*V*, *I*, bq_{ANS}	74.1	71.2	0.162	***−0.021***	0.053	0.000 (−0.310)	62.16	no
am_9	*V*, bq_{ANS}, η	74.1	71.1	0.129	***−0.019***	***0.034***	0.000 (−0.310)	62.36	no
am_{10}	*V*, bq_{ANS}, PA	72.0	68.7	0.217	***−0.059***	0.072	−0.238 (−0.310)	55.27	no

[a] R^2. [b] R_{adj}^2. [c] $K_{XY} - K_X > \delta K = 0.1$. [d] $Q_{LOO}^2 - Q_{ASYM}^2 > \delta Q = 0$. [e] $t^P > R^P = 0.05$. [f] $R^N > t^N(0.02)$. [g] $Q_{boot} > 50\%$.

heterocyclic molecules on the inhibition corrosion efficiency by means of an univariate linear regression model (Figure 2); the results showed that the correlation coefficients are smaller than 0.6, i.e., there are no single linear correlations statistically acceptable. Nevertheless, from the scatter plots it can be seen that the eff % displayed a rough correlation with some properties such as molecular volume, ionization potential, and anisotropy (Figure 2). These results prompted us to explore another approach based on multiple linear correlations, in particular a QSPR model.

A key step in the process to obtain a reliable QSPR model is the determination of a correlation matrix of the calculated descriptors whose goal is to avoid multicollinearity;[32,33] the results, summarized in Table 3, showed possible pairwise correlation coefficients for a given set of descriptors. From the correlation matrix, we observed that some descriptors showed some degree of redundancy. For instance, hardness showed correlation coefficients equal or greater than 0.5 with Log *P*, *V*, HOMA, ω, ω^-, *I*, and *A*. A thumb rule in a correlation model is that a descriptor that shows high correlation might not be present because the redundant values with positive contributions generates a nonreliable equation with overestimated statistical data.

QSPR Models. Multiple linear regression analysis was employed for searching the optimal QSPR models in both gas (gm_i) and aqueous (am_i) phases (i = 1−10) to identify the

DOI: 10.1021/acs.jcim.5b00385
J. Chem. Inf. Model. 2015, 55, 2391−2402

essential parameters involved in the corrosion inhibition (Tables 4 and 5). The models were validated by means of several statistical parameters[32−35] including leave one-out cross-validation Q_{LOO}^2, squared correlation coefficient (R^2), squared correlation adjusted coefficient (R_{adj}^2), the QUIK rule (δK) based on the K multivariate correlation index, the asymptotic Q^2 rule (δQ), R^P, and R^N. The last two indices have been used to detect models with an excess of *good* predictors (R^P) as well as models with an excess of *bad* predictors (R^N).[32] In addition, a Q_{F3}^2 rule was used for predictions of external test objects.[34,35]

Initially, we selected the first ten models for each phase displaying the largest calculated values of R^2 ($R^2 > 66.4$, Table 4 and 5). Second, we applied the QUIK rule with a threshold equal to 0.1; this rule is a simple criterion that allows the rejection of models with high predictor collinearity and it has been very effective in avoiding models with multicollinearity without prediction power. From the data, it can be seen that the gm_1, gm_2, gm_3, gm_4, gm_5, gm_9, am_1, am_3, and am_4 models did not fulfill the QUIK rule with the threshold selected ($\delta K = 0.1$).

Then, an additional criterion was considered to select the best regression model. The criterion was based on the asymptotic behavior of Q^2 which determines the prediction capability of the model.[80,81] We used the $Q_{LOO}^2 - Q_{ASYM}^2 < \delta Q$ rule, the chosen value was 0.0. Hence, by applying this rule, models gm_7, gm_{10}, and am_1 to am_{10} were rejected, leaving gm_8 as the only one that fulfills this criterion, in addition to the rules R^P and R^N that are used to detect models with an excess of good and bad predictors.

The best QSPR model gm_8 (Table 4) is given by eq 12. This QSPR model highlights the correlation between the eff % with structural parameters, electronic properties, and aromaticity of the 25 heterocyclic molecules for training as well as the five molecules to test.

$$\text{eff\%} = 92.965 + 0.152V + 35.337\omega^- + 3.592\text{bq}_{ANS} \quad (12)$$

where eff % = corrosion inhibition efficiency; V = volume (Å^3); ω^- = electron donor capability (eV); bq_{ANS} = anisotropy (dimensionless units).

The statistical data derived from the equation are $R^2 = 75.06$, $R_{adjusted}^2 = 71.49$, $F = 21.1$, $Q_{boot} = 61.83$, $\delta K = 0.183$, $\delta Q = 0.001$, $R^P = 0.094$, and $R^N = 0.000$ (−0.310). This model fulfills all the statistic validation rules[80,81] such as $R^2 > 60$ and $Q^2 > 50$. According to eq 12, the corrosion inhibition is influenced by the molecular volume V, by the electron donor capability ω^-, a measure of the fractionate charge transfer of a molecule, and by the anisotropy bq_{ANS}, that is considered as an aromaticity index. It is worthwhile to mention that descriptors such as molecular volume or $E_{LUMO} - E_{HOMO}$ gap have been recognized as relevant in the field of corrosion inhibition.[82] In connection to this, we studied the interaction of an iron surface with two heterocyclic molecules possessing the basic backbone displayed by the molecules studied with the intention to gain further insight into the role of these descriptors on the corrosion inhibition (*vide infra*).

Model Validation: Electrochemical Studies. In order to calibrate and validate the QSPR model, we experimentally examined by EIS the corrosion behavior of carbon steel in acidic media 1.0 M HCl in the presence of six heterocyclic compounds, namely; imidazole, 2-methylimidazole, benzimidazole, 2-chloromethylbenzimidazole, pyridine, and 2-aminopyridine. The imidazole and benzimidazole compounds were used to reproduce experimental results previously reported.[74] The last two molecules that are not included in the QSPR model, were left out to validate the model. The Nyquist plots for the six different inhibitors as well as the control experiment are shown in Figure 3.

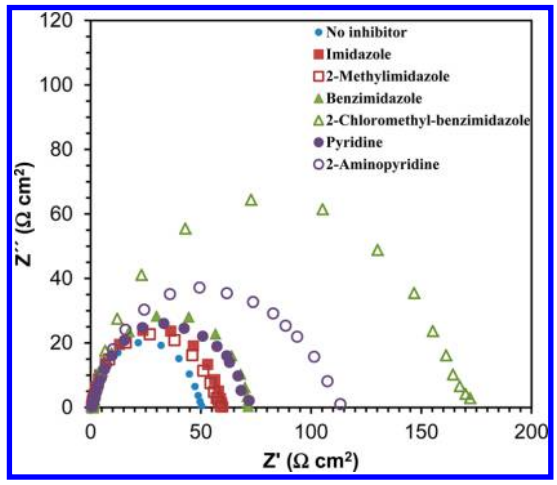

Figure 3. Nyquist plots of carbon steel in 1.0 M HCl without and with heterocyclic compounds used as inhibitors (10^{-3} M).

The Nyquist plots displayed a single semicircle shifted along the real impedance axis (Z'), indicating that corrosion of carbon steel in 1.0 M HCl is controlled by a charge-transfer[82,83] process; the diameter of the capacitive loop increases in the presence of the inhibitors. This increase in the charge transfer resistance (R_{ct}) value can be attributed to the formation of a protective film on the metal solution interface.[63]

Experimental corrosion inhibition efficiency values were calculated according to the eq 1; the values are shown in the Table 6 and are consistent with those reported in the literature.[74]

Table 6. Descriptors Calculated with PBE/6-311++G and Corrosion Inhibition Efficiency (eff %)**

compounds	V	ω^+	bq_{ANS}	eff %[a]	eff %[b]
imidazole	89	0.09	−27.19	12.55	12.4
2-methylimidazole	116	0.16	−28.16	13.90	15.9
benzimidazole	150	0.25	−27.47	26.64	26.4
2-chloromethylbenzimidazole	198	0.30	−21.97	69.70	54.8
pyridine	113	0.29	−26.81	27.17	24.1
2-aminopyridine	131	0.30	−21.07	51.25	48.1

[a]Obtained by EIS in this work. [b]Calculated with our model (eq 12).

The observed and predicted values for corrosion inhibition were plotted (Figure 4); these data showed an acceptable goodness of fit. The external predictive ability was calculated with $Q_{F3}^2 = 0.987$, a function widely used for external testing.[34,35] From the plot it can be observed that 2-chloromethylbenzimidazole is a better corrosion inhibitor than the other compounds. These results clearly attest that the mathematical QSPR model (eq 12) represents a highly efficient approach to predict the corrosion inhibition of either pyridine- or imidazole-based compounds.

In order to further test the reliability of our QSPR model (eq 12), we extended our calculations on the corrosion inhibition ability to other related compounds such as quinoline derivatives.[7] By means of the application of our model (eq

DOI: 10.1021/acs.jcim.5b00385
J. Chem. Inf. Model. 2015, 55, 2391−2402

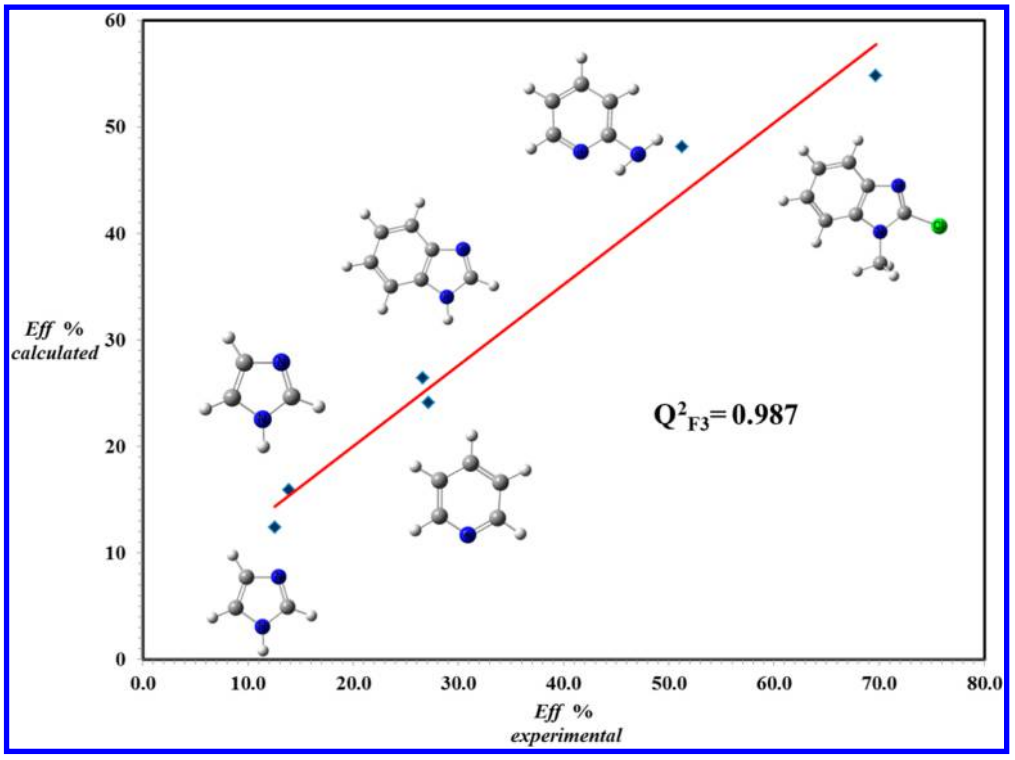

Figure 4. Experimental corrosion inhibition percentage versus calculated corrosion inhibition percentage from eq 12.

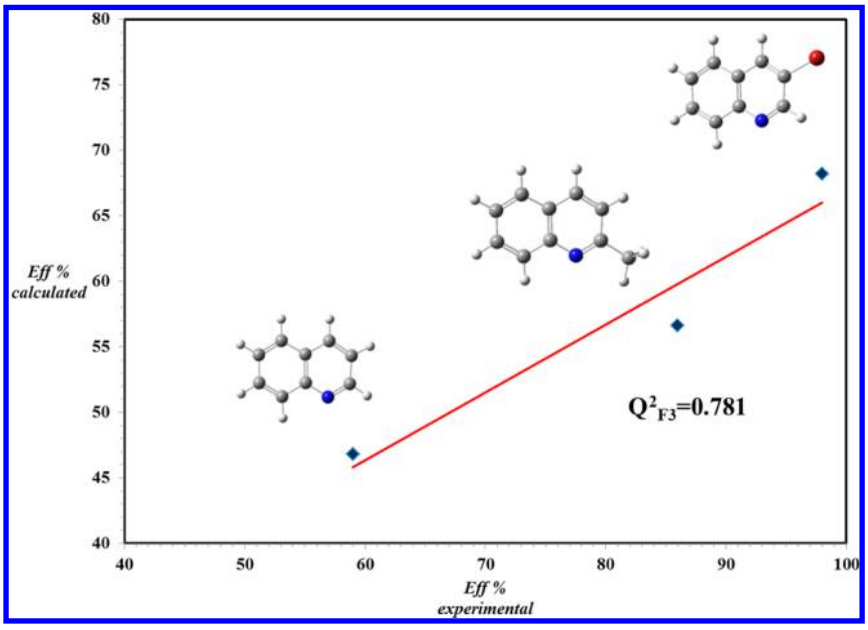

Figure 5. Reported[7] versus calculated corrosion inhibition percentages for quinoline derivatives.

12) with a Q_{F3}^2 = 0.781, we calculated eff % values of 46.8, 56.6, and 68.2 for quinoline, 2-methyl-quinoline, and 3-bromoquinoline respectively; these results are in excellent agreement with the experimental data for these compounds, previously reported (Figure 5).

Adsorption Interactions. With the intention to asses additional insights into the interaction and mechanism aspects of corrosion inhibition, we performed DFT calculations to model the adsorption behavior of imidazole and benzimidazole molecules onto a Fe(110) surface in aqueous solution, as representative cases of this family of nitrogenate heterocycles. Our results predict that imidazole and benzimidazole molecules are adsorbed on hollow and top sites of the Fe(110) surface. Initially, we considered the approaching of the heterocycles to iron surface in either a parallel or perpendicular arrangement; the most stable array involves the molecular approaching in the parallel stacking-like fashion. Then, several interaction modes between a given Fe atom and the inhibitor molecules were considered. In one scenario, the iminic-type nitrogen is placed directly above of a Fe atom, thus allowing a full geometry optimization; the most favorable adsorption modes for imidazole and benzimidazole are depicted in Figure 6.

The N−Fe average distances were 1.98 Å for imidazole and 2.17 Å for benzimidazole; these distances are close to the sum

DOI: 10.1021/acs.jcim.5b00385
J. Chem. Inf. Model. 2015, 55, 2391−2402

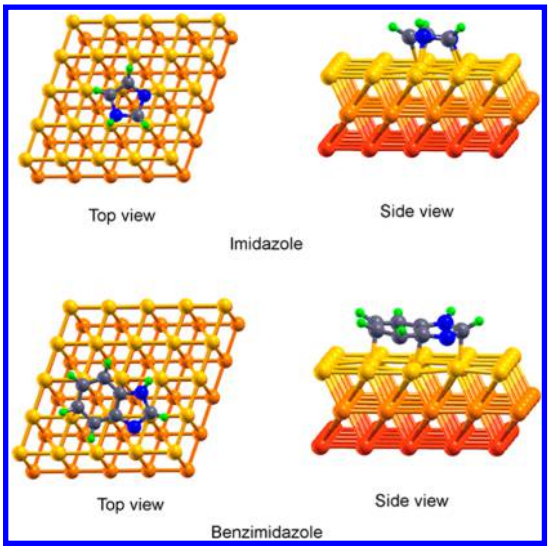

Figure 6. Adsorption geometries of imidazole and benzimidazole on the Fe(110) surface in aqueous solution.

of the covalent radii [$\sum r_{cov}$(Fe, N) = 1.95 Å].[84] The averaged Fe−C bond distances for both molecules were 2.10 Å, and they are close to the covalent radii sum [$\sum r_{cov}$(Fe, C) = 1.97 Å]. These data are indicative of an effective interaction between the five-membered heterocyclic ring and the iron surface. In connection to this, the $\pi \rightarrow$ d charge transfer calculated by means of Bader's method (molecule → surface) was 0.80 and 0.97 for imidazole and benzimidazole, respectively; this outcome also supported the existence of the heterocycle/Fe(110) interaction.

Furthermore, the adsorption energies were calculated according to eq 9. The adsorption energies were −23.38 and −27.63 kcal/mol for imidazole and benzimidazole in vacuum, respectively; in aqueous solution, the adsorption energies were −30.48 and −36.29 kcal/mol for imidazole and benzimidazole, respectively. These data strongly suggests that the corrosion inhibition of benzimidazole is larger between these two molecules; this result is fully consistent with the experimental values and with our proposed mathematical model.

CONCLUSIONS

We have developed a reliable mathematical model able to predict with high efficiency the corrosion-inhibition attributes of nitrogen-based heterocyclic inhibitors. The model takes into account the volume, electron donor capability and anisotropic descriptors. This mathematical approach was validated by comparing the theoretical results based on 30 molecules previously reported with the experimental corrosion data of representative nitrogenate heterocycles (imidazole, 2-methyl-imidazole, benzimidazole, 2-chloromethylbenzimidazole, pyridine, and 2-aminopyridine), that we measured in this work by electrochemical impedance spectroscopy. The model predicts that the efficiency of 2-chloromethyl-benzimidazole is higher than that of benzimidazole as corroborated by the experimental results and, thus, proving that this model is an efficient tool to predict the properties of corrosion inhibitors. The adsorption studies of imidazole and benzimidazole molecules onto the Fe(110) surface predicted that benzimidazole could be a better inhibitor than imidazole based on their adsorption energies. These results suggest that aromaticity would play a fundamental role in the formation of the adsorbate−surface complex; in this sense, the Fe−C interaction may be a key step in the mechanism of corrosion inhibition. This proposal is consistent with our mathematical approach which also considers the anisotropy (bq_{ANS}), an aromaticity index, for the calculations (eq 12).

Our results provide valuable insights into the interaction mechanism of nitrogenate-heterocyclic inhibitors and the relationship between their electronic-molecular properties and their corrosion-inhibition ability. We envisaged that this mathematical approach may be extended to the study of other family of compounds in the context of corrosion inhibition, as an efficient method to provide advantageous considerations for the rational design and engineering of novel materials to inhibit corrosion.

ASSOCIATED CONTENT

Supporting Information

The Supporting Information is available free of charge on the ACS Publications website at DOI: 10.1021/acs.jcim.5b00385.

Tables S1a−S1c: geometrical parameters such as bond distances and bond angles in our systems. Tables S2a−S2e: descriptors calculated with all methods (PDF)

AUTHOR INFORMATION

Corresponding Author

*E-mail: jcruz@uaeh.edu.mx. Phone: +52 771 71 72000 ×2210. Fax: +52 771 71 72000 ×6502.

Notes

The authors declare no competing financial interest.

ACKNOWLEDGMENTS

R.L.C.-M. acknowledges CONACyT for her fellowship. J.C.-B. acknowledges financial support from CONACyT (Project 106474). We gratefully acknowledge the Dirección General de Cómputo y de Tecnologías de Información y Comunicación (DGCTIC) at the Universidad Nacional Autónoma de México and the Laboratorio de Visualización y Cómputo Paralelo at UAM—Iztapalapa for the computer facilities.

REFERENCES

(1) Obot, I. B.; Macdonald, D.; Gasem, Z. M. Density functional theory (DFT) as a powerful tool for designing new organic corrosion inhibitors. Part 1: An overview. *Corros. Sci.* **2015**, *99*, 1.

(2) Behzadi, H.; Roonasi, P.; Momeni, M. J.; Manzetti, S.; Esrafili, M. D.; Obot, I. B.; Yousefvand, M.; Mousavi-Khoshdel, S. M. A DFT study of pyrazine derivatives and their Fe complexes in corrosion inhibition process. *J. Mol. Struct.* **2015**, *1086*, 64−72.

(3) Obot, I. B.; Umoren, S. A.; Gasem, Z. M.; Suleiman, R.; El Ali, B. Theoretical Prediction and electrochemical evaluation of vinylimidazoline and allylimidazoline as corrosion inhibitors for mild steel in 1 M HCl. *J. Ind. Eng. Chem.* **2015**, *21*, 1328−1339.

(4) Kabanda, M. M.; Obot, I. B.; Ebenso, E. E. Computational Study of Some Amino Acid Derivatives as Potential Corrosion Inhibitors for Different Metal Surfaces and in Different Media. *Int. J. Electrochem. Sci.* **2013**, *8*, 10839−10850.

(5) Obot, I. B.; Ebenso, E. E.; Kabanda, M. M. Metronidazole as environmentally safe corrosion inhibitor for mild steel in 0.5 M HCl: Experimental and theoretical investigation. *J. Environ. Chem. Eng.* **2013**, *1* (3), 431−439.

(6) Jovancicevic, V.; Ramachandran, S.; Prince, P. Inhibition of Carbon Dioxide of Mild Steel by Imidazolines and their precursors. *Corrosion* **1999**, *55*, 449−455.

DOI: 10.1021/acs.jcim.5b00385
J. Chem. Inf. Model. 2015, 55, 2391−2402

(7) Lukovits, I.; Kalmán, E.; Zucchi, F. Corrosion Inhibitors Correlation Between Electronic Structure an Efficiency. *Corrosion* **2001**, *57*, 3−8.
(8) Bentiss, F.; Lagrenee, M.; Traisnel, M.; Hornez, J. C. The corrosion inhibition of mild steel in acidic media by a new triazole derivative. *Corros. Sci.* **1999**, *41*, 789−803.
(9) Cruz, J.; Martínez, L. M. R.; Salcedo, R.; Castro, M. Reactivity Properties of Derivatives of 2-Imidazoline: An ab initio DFT Study. *Int. J. Quantum Chem.* **2001**, *85*, 546−556.
(10) Cruz, J.; Garcia, E.; Castro, M. Experimental and Theoretical Study of the 3-Amino-1,2,4-triazole and 2-Aminothiazole Corrosion Inhibitors in Carbon Steel. *J. Electrochem. Soc.* **2003**, *150*, 26−35.
(11) Cruz, J.; Martínez, R.; Genesca, J.; García-Ochoa, E. Experimental and theoretical study of 1-(2-ethylamino)-2 methyl-imidazoline as an inhibitor of carbon steel corrosion in acid media. *J. Electroanal. Chem.* **2004**, *566*, 111−121.
(12) Cruz, J.; Pandiyan, T.; García, E. A new inhibitor for mild carbon steel: Electrochemical and DFT studies. *J. Electroanal. Chem.* **2005**, *583*, 8−16.
(13) Turcio-Ortega, D.; Pandiyan, T.; Cruz, J.; Garcia, E. Interaction of Imidazoline Compounds with Fen (n) 1−4 Atoms as a Model for Corrosion Inhibition: DFT and Electrochemical Studies. *J. Phys. Chem. C* **2007**, *111*, 9853−9866.
(14) Roque, J. M.; Pandiyan, T.; Cruz, J.; García, E. DFT and electrochemical studies of tris(benzimidazole-2-ylmethyl)amine as an efficient corrosion inhibitor for carbon steel surface. *Corros. Sci.* **2008**, *50*, 614−624.
(15) Camacho, R. L.; Montiel, E.; Jayanthi, N.; Pandiyan, T.; Cruz, J. DFT studies of a-diimines adsorption over Fen surface (n = 1, 4, 9 and 14) as a model for metal surface coating. *Chem. Phys. Lett.* **2010**, *485*, 142−151.
(16) Berhanu, W. M.; Pillai, G. G.; Oliferenko, A. A.; Katritzky, A. R. Quantitative structure−activity/property relationships: The ubiquitous links between cause and effect. *ChemPlusChem* **2012**, *77* (7), 507−517.
(17) Medina-Franco, J. L.; Navarrete-Vázquez, G.; Méndez-Lucio, O. Property Landscape Modeling is at the Interface of Chemoinformatics and Experimental Sciences. *Future Med. Chem.* **2015**, *7*, 1197−1211.
(18) Selwood, D. L.; Livingstone, D. J.; Comley, J. C. W.; O'Dowd, A. B.; Hudson, T.; Jackson, P.; Jandu, K. S.; Rose, V. S.; Stables, J. N. Structure- Activity Relationships of Antifilarial Antimycin Analogues: A Multivariate Pattern Recognition Study. *J. Med. Chem.* **1990**, *33*, 136−142.
(19) Sharma, B. K.; Singh, P.; Prabhakar, Y. S. QSAR Rationale of Matrix Metalloproteinase Inhibition Activity in a Class of Carboxylic Acid Based Compounds. *Br. J. Pharm. Res.* **2013**, *3* (4), 697−721.
(20) Nandy, A.; Kar, S.; Roy, K. Development and validation of regression-based QSAR models for quantification of contributions of molecular fragments to skin sensitization potency of diverse organic chemicals. *SAR and QSAR in Enviromental Research.* **2013**, *24* (12), 1009−1023.
(21) George, F. G.; Ismail, S. M. I.; Stawinski, J.; Girgis, A. S. Design, Synthesis and QSAR studies of dispiroindole derivatives as new antiproliferative agents. *Eur. J. Med. Chem.* **2013**, *68*, 339−351.
(22) Bhhatarai, B.; Gramatica, P. Modelling physico-chemical properties of (benzo)triazoles, and screening for environmental partitioning. *Water Res.* **2011**, *45*, 1463−1471.
(23) Taboureau, O. Methods for Building Quantitative Structure−Activity Relationship (QSAR) Descriptors and Predictive Models for Computer-Aided Design of Antimicrobial Peptides. *Methods Mol. Biol.* **2010**, *618*, 77−86.
(24) Zhu, M.; Ge, F.; Zhu, R.; Wang, X.; Zheng, X. A DFT-based QSAR study of the toxicity of quaternary ammonium compounds on Chlorella vulgaris. *Chemosphere* **2010**, *80*, 46−52.
(25) Ruggiu, F.; Gizzi, P.; Galzi, J. L.; Hibert, M.; Haiech, J.; Baskin, I.; Horvath, D.; Marcou, G.; Varnek, A. Quantitative Structure-Property Relationship Modeling. A valuable support in High − Throughput Screening Quality Control. *Anal. Chem.* **2014**, *86*, 2510−2520.
(26) Cox, R.; Green, D. V. S.; Luscombe, C. N.; Malcolm, N.; Pickett, S. D. QSAR workbench: automating QSAR modeling to drive compound design. *J. Comput.-Aided Mol. Des.* **2013**, *27*, 321−336.
(27) Duchowicz, P. R.; Mirífico, M. V.; Rozas, M. F.; Caram, J. A.; Fernández, F. M.; Castro, E. A. Quantitative structure−spectral property relationships for functional groups of novel 1,2,5-thiadiazole compounds. *Chemom. Intell. Lab. Syst.* **2011**, *105*, 27−37.
(28) Zhang, S. G.; Lei, W.; Xia, M. Z.; Wang, F. Y. QSAR study on N-containing corrosion inhibitors: Quantum chemical approach assisted by topological index. *J. Mol. Struct.: THEOCHEM* **2005**, *732*, 173−182.
(29) Glossman-Mitnik, D. CBS-QB3 calculation of quantum chemical molecular descriptors of isomeric thiadiazoles. *J. Mol. Graphics Modell.* **2006**, *25*, 455−458.
(30) El Ashry, El S. H.; Senior, S. A. QSAR of lauric hydrazide and its salts as corrosion inhibitors by using the quantum chemical and topological descriptors. *Corros. Sci.* **2011**, *53*, 1025−1034.
(31) Khaled, K. F. Modeling corrosion inhibition of iron in acid medium by genetic function approximation method: A QSAR model. *Corros. Sci.* **2011**, *53*, 3457−3465.
(32) Todeschini, R.; Consonni, V.; Mauri, A.; Pavan, M. Detecting "bad" regresion models: multicriteria fitness functions in regression analysis. *Anal. Chim. Acta* **2004**, *515*, 199−208.
(33) *Mobydigs−Software for Multilinear Regression Analysis and Variable Selection by Genetic Algorithm*, version 1.0 for Windows; Milano Chemometrics and QSAR Research Group: Milano, Italy, 2006.
(34) Consonni, V.; Ballabio, D.; Todeschini, R. Comments on the Definition of the Q2 Parameter for QSAR Validation. *J. Chem. Inf. Model.* **2009**, *49*, 1669−1678.
(35) Consonni, V.; Ballabio, D.; Todeschini, R. Evaluation of model predictive ability by external validation techniques. *J. Chemom.* **2010**, *24*, 194−201.
(36) Fodor, C.; Kali, G.; Iván, B. Poly(N-vinylimidazole)-I-Poly-(tetrahydrofuran) amphiphilic conetworks and gels: Synthesis, characterization, thermal and swelling behavior. *Macromolecules* **2011**, *44*, 4496−4502.
(37) Samanta, S.; Das, S.; Biswas, P. Photocatalysis by 3,6-Disubstituted-s-Tetrazine: Visible-Light Driven Metal-Free Green Synthesis of 2- Substitued Benzimidazole and Benzothiazole. *J. Org. Chem.* **2013**, *78*, 11184−11193.
(38) Yoo, S. H.; Kim, Y. W.; Chung, K.; Baik, S. Y.; Kim, J. S. Synthesis and corrosion inhibition behavior of imidazoline derivates based on vegetable oil. *Corros. Sci.* **2012**, *59*, 42−54.
(39) Rani, B. E. A.; Basu, B. B. J. Green inhibitors for corrosion protection of metals and alloys: an overview. *Int. J. Corros.* **2012**, *2*, 1−15.
(40) Kliskic, M.; Radosevi, J.; Gudic, S. Pyridine and its derivatives as inhibitors of aluminium corrosion in chloride solution. *J. Appl. Electrochem.* **1997**, *27*, 947−952.
(41) Perdew, J. P.; Burke, K.; Ernzerhof, M. Generalized Gradient Approximation Made Simple. *Phys. Rev. Lett.* **1996**, *77*, 3865−3868.
(42) Perdew, J. P.; Burke, K.; Ernzerhof, M. Generalized Gradient Approximation Made Simple. *Phys. Rev. Lett.* **1997**, *78*, 1396.
(43) Becke, A. D. Density-functional thermochemistry. III. The role of exact exchange. *J. Chem. Phys.* **1993**, *98*, 5648−5652.
(44) Zhao, Y.; Truhlar, D. G. The M06 suite of density functionals for main group thermochemistry, thermochemical kinetics, noncovalent interactions, excited states, and transition elements: two new functionals and systematic testing of four M06-class functionals and 12 other functionals. *Theor. Chem. Acc.* **2008**, *120*, 215−241.
(45) Frisch, M. J.; Trucks, G. W.; Schlegel, H. B.; Scuseria, G. E.; Robb, M. A.; Cheeseman, J. R.; Scalmani, G.; Barone, V.; Mennucci, B.; Petersson, G. A.; Nakatsuji, H.; Caricato, M.; Li, X.; Hratchian, H. P.; Izmaylov, A. F.; Bloino, J.; Zheng, G.; Sonnenberg, J. L.; Hada, M.; Ehara, M.; Toyota, K.; Fukuda, R.; Hasegawa, J.; Ishida, M.; Nakajima, T.; Honda, Y.; Kitao, O.; Nakai, H.; Vreven, T.; Montgomery, J. A., Jr.; Peralta, J. E.; Ogliaro, F.; Bearpark, M.; Heyd, J. J.; Brothers, E.; Kudin, K. N.; Staroverov, V. N.; Kobayashi, R.; Normand, J.; Raghavachari, K.;

DOI: 10.1021/acs.jcim.5b00385
J. Chem. Inf. Model. 2015, 55, 2391−2402

Rendell, A.; Burant, J. C.; Iyengar, S. S.; Tomasi, J.; Cossi, M.; Rega, N.; Millam, J. M.; Klene, M.; Knox, J. E.; Cross, J. B.; Bakken, V.; Adamo, C.; Jaramillo, J.; Gomperts, R.; Stratmann, R. E.; Yazyev, O.; Austin, A. J.; Cammi, R.; Pomelli, C.; Ochterski, J. W.; Martin, R. L.; Morokuma, K.; Zakrzewski, V. G.; Voth, G. A.; Salvador, P.; Dannenberg, J. J.; Dapprich, S.; Daniels, A. D.; Farkas, Ö.; Foresman, J. B.; Ortiz, J. V.; Cioslowski, J.; Fox, D. J. *Gaussian 09*, Revision D.01; Gaussian, Inc.: Wallingford, CT, 2010.

(46) Camacho-Mendoza, R. L.; Aquino-Torres, E.; Cruz-Borbolla, J.; Alvarado-Rodriguez, J. G.; Olvera-Neria, O.; Narayanan, J.; Pandiyan, T. DFT analysis: Fe_4 cluster and Fe(110) surface interaction studies with pyrrole, furan, thiophene, and selenophene molecules. *Struct. Chem.* **2014**, *25*, 115−126.

(47) Stanger, A. Nucleus Independent Chemical Shifts (NICS): Distance Dependence and Revised Criteria for Aromaticity and Antiaromaticity. *J. Org. Chem.* **2006**, *71*, 883−893.

(48) Fallah-Bagher-Shaidaei, H.; Wannere, Ch. S.; et al. Which NICS Aromaticity Index for Planar p Rings Is Best? *Org. Lett.* **2006**, *8*, 863−866.

(49) (a) Biegler-König, F.; Bayles, D.; Schönbohm, J. *AIM 2000* Version 1.0; University of Applied Sciences, Bielefeld, Germany, 1998−2000. (b) Krygowski, T. M. Crystallographic studies of inter- and intramolecular interactions reflected in aromatic character of.pi.-electron systems. *J. Chem. Inf. Model.* **1993**, *33*, 70−78.

(50) Lu, T.; Chen, F. Multiwfn: A Multifunctional Wavefunction Analyzer. *J. Comput. Chem.* **2012**, *33*, 580−592.

(51) Krygowski, T. M.; Cyranski, M. K.; Czarnocki, Z.; Hafelinger, G.; Katritzky, A. R. Aromaticity: a Theoretical Concept of Immense Practical Importance. *Tetrahedron* **2000**, *56*, 1783−1796.

(52) Kresse, G.; Furthmüller, J. Efficient iterative schemes for ab initio total-energy calculations using a plane-wave basis set. *Phys. Rev. B: Condens. Matter Mater. Phys.* **1996**, *54*, 11169−11186.

(53) Kresse, G.; Furthmüller, J. Efficiency of ab-initio total energy calculations for metals and semiconductors using a plane-wave basis set. *Comput. Mater. Sci.* **1996**, *6*, 15−50.

(54) Blöchl, P. E. Projector Augmented-Wave Method. *Phys. Rev. B: Condens. Matter Mater. Phys.* **1994**, *50*, 17953−17979.

(55) Kresse, G.; Joubert, D. From Ultrasoft Pseudopotentials to the Projector Augmented-Wave Method. *Phys. Rev. B: Condens. Matter Mater. Phys.* **1999**, *59*, 1758−1775.

(56) Jiang, D. E.; Carter, E. A. First principles study of H_2S adsorption and dissociation on Fe(1 1 0). *Surf. Sci.* **2005**, *583*, 60−68.

(57) Freitas, R. R. Q.; Rivelino, R.; Brito Mota, F.; Castilho, C. M. C. Dissociative Adsorption and Aggregation of Water on the Fe(100) Surface: A DFT Study. *J. Phys. Chem. C* **2012**, *116*, 20306−20314.

(58) Bader, R. F. W.; Beddall, P. M. Virial Field Relationship for Molecular Charge Distributions and the Spatial Partitioning of Molecular Properties. *J. Chem. Phys.* **1972**, *56*, 3320−3330.

(59) Bader, R. F. W. A Quantum Theory of Molecular Structure and Its Applications. *Chem. Rev.* **1991**, *91*, 893−928.

(60) Wu, S. Y.; Su, C. H.; Chang, J. G.; Chen, H. T.; Hou, C. H.; Chen, H. L. Adsorption and dissociation of N_2O molecule on Fe(111) surface: A DFT study. *Comput. Mater. Sci.* **2011**, *50*, 3311−3314.

(61) Mathew, K.; Sundararaman, R.; Letchworth-Weaver, K.; Arias, T. A.; Hennig, R. G. Implicit solvation model for density-functional study of nanocrystal surfaces and reaction pathways. *J. Chem. Phys.* **2014**, *140*, 084106.

(62) Chidiebere, M. A.; Oguzie, E. E.; Liu, L.; Li, Y.; Wang, F. Ascorbic acid as corrosion inhibitor for Q235 mild steel in acidic environments. *J. Ind. Eng. Chem.* **2015**, *26*, 182−192.

(63) Chauhan, L. R.; Gunasekaran, G. Corrosion inhibition of mild steel by plant extract in dilute HCl medium. *Corros. Sci.* **2007**, *49*, 1143−1161.

(64) De Proft, F.; Van Alsenoy, C.; Peeters, A. W.; Langenaeker, P.; et al. Geerlings, Atomic charges, dipole moments, and Fukui functions using the Hirshfeld partitioning of the electron density. *J. Comput. Chem.* **2002**, *23*, 1198−1209.

(65) Szabo, A.; Ostlund, N. S. *Modern Quantum Chemistry: Introduction to Advanced Electronic Structure Theory*; Dover Books on Chemistry/Dover Publications: Mineola, NY, 1989.

(66) Parr, R. G.; Donnelly, R. A.; Levy, M.; Palke, W. E. Electronegativity- the density functional viewpoint. *J. Chem. Phys.* **1978**, *68*, 3801−3807.

(67) Pearson, R. G. Absolute electronegativity and hardness: application to inorganic chemistry. *Inorg. Chem.* **1988**, *27*, 734−740.

(68) Pearson, R. G. Principle of Maximum Physical Hardness. *J. Phys. Chem.* **1994**, *98*, 1989−1992.

(69) Gázquez, J. L.; Cedillo, A.; Vela, A. Electrodonating and Electroaccepting Powers. *J. Phys. Chem. A* **2007**, *111*, 1966−1970.

(70) Avelar, M.; Martinez, A. Do Caseiopeinas prevent cancer disease by acting as antiradicals? A chemical reactivity study applying Density Functional Theory. *J. Mex. Chem. Soc.* **2012**, *56*, 250−256.

(71) Valencia, D.; Klimova, T.; García-Cruz, I. Aromaticity of five- and six-membered heterocycles presesent in crude oils and electronic description for hydrotreatment process. *Fuel* **2012**, *100*, 177−185.

(72) Sha, Y.; Yu, T. H.; Liu, Y.; Merinov, B. V.; Goddard, W. A. Theoretical study of solvent effects on the platinum-catalyzed oxygen reduction reaction. *J. Phys. Chem. Lett.* **2010**, *1*, 856−861.

(73) Yin, W. J.; Krack, M.; Wen, B.; Ma, S. Y.; Liu, L. M. CO_2 capture and conversion on rutile TiO_2(110) in the water environment: insight by first-principles calculations. *J. Phys. Chem. Lett.* **2015**, *6*, 2538−2545.

(74) Raicheva, S. N.; Aleksiev, B. V.; Sokolova, E. I. The effect of the chemical structure of some nitrogen and sulphur containing organic compounds on their corrosion inhibiting action. *Corros. Sci.* **1993**, *34*, 343−350.

(75) Hachula, B.; Nowak, M.; Kusz, J. Crystal and Molecular Structure Analysis of 2-Methylimidazole. *J. Chem. Crystallogr.* **2010**, *40*, 201−206.

(76) Fahrni, C. J.; Henary, M. M.; Van Derveer, D. G. Excited-State Intramolecular Proton Transfer in 2-(2′Tosylaminophenyl)-benzimidazole. *J. Phys. Chem. A* **2002**, *106*, 7655−7663.

(77) Borba, A.; Zavaglia, A. G.; Fausto, R. Molecular Structure, Vibrational Spectra, Quantum Chemical Calculations and Photochemistry of Picolinamide and Isonicotinamide Isolated in Cryogenic Inert Matrixes and in the Neat Low-Temperature Solid Phases. *J. Phys. Chem. A* **2008**, *112*, 45−57.

(78) Amin, M. A.; Ahmed, M. A.; Kandemirli, F.; Saracoglu, M.; Arslan, T.; Basaran, M. A.; Arida, H. A. Monitoring corrosion and corrosion control of iron in HCl by non-ionic surfactants of the TRITON-X series − Part III. Immersion time effects and theoretical studies. *Corros. Sci.* **2011**, *53*, 1895−1909.

(79) Sastri, V. S.; Perumareddi, J. R. Molecular Orbital Theoretical Studies of Some Organic Corrosion Inhibitors. *Corrosion* **1997**, *53*, 617−622.

(80) Golbraikh, A.; Tropsha, A. Beware of q^2! *J. Mol. Graphics Modell.* **2002**, *20*, 269−276.

(81) Tropsha, A.; Gramatica, P.; Gombar, V. K. The importance of being earnest: Validation is the absolute essential for successful application and interpretation of QSPR models. *QSAR Comb. Sci.* **2003**, *22*, 69−77.

(82) Goulart, C. M.; Esteves-Souza, A.; Martinez-Huitle, C. A.; Rodrigues, C. J.; Maciel, M. A.; Echevarria, A. Experimental and theoretical evaluation of semicarbazones and thiosemicarbazones as organic corrosion inhibitors. *Corros. Sci.* **2013**, *67*, 281−291.

(83) Mansfeld, F. Use of electrochemical impedance spectroscopy for the study of corrosion protection by polymer coatings. *J. Appl. Electrochem.* **1995**, *25*, 187−202.

(84) Porterfield, W. W. *Inorganic Chemistry: A Unified Approach*; Addison-Wesley: Reading, MA, 1984.

DOI: 10.1021/acs.jcim.5b00385
J. Chem. Inf. Model. 2015, 55, 2391−2402